A&A 399, 169–175 (2003)
DOI: 10.1051/0004-6361:20021798

Astronomy & Astrophysics

Stringent upper limits to the solid NH_3 abundance towards W 33A from near-IR spectroscopy with the Very Large Telescope⋆

I. M. Taban[1], W. A. Schutte[1], K. M. Pontoppidan[2], and E. F. van Dishoeck[1,2]

[1] Raymond and Beverly Sackler Laboratory for Astrophysics, Leiden Observatory, PO Box 9513, 2300 RA Leiden, The Netherlands
[2] Leiden Observatory, PO Box 9513, 2300 RA Leiden, The Netherlands

Received 19 September 2002 / Accepted 14 November 2002

Abstract. We obtained near-infrared spectroscopy of the high mass young stellar object W 33A between 1.9–2.5 μm in search of absorption features of circumstellar ices. The 2.27 μm band of CH_3OH is positively identified in the spectrum, its intensity being fully consistent with the column density derived earlier from the methanol bands at 3.54 and 3.91 μm. The 2.21 μm band of solid NH_3, on the other hand, was not detected. This shows that the quantity of solid NH_3 towards W 33A is at least 3 times lower than earlier estimates based on the NH_3 umbrella mode at 9 μm.

Key words. methods: laboratory – stars: individual: W 33A – ISM: abundances – ISM: molecules – infrared: ISM – ISM: lines and bands

1. Introduction

While, at least for the general dense medium, the total oxygen and carbon budget seems to be rather well accounted for (Schutte 1999), the nature of the gaseous and icy carriers of the nitrogen is still quite unclear. Ammonia (NH_3) could be an important nitrogen carrying component of interstellar ices. It forms when atomic nitrogen is reduced by atomic hydrogen on the surfaces of dust particles (Hiraoka et al. 1995). Furthermore, NH_3 could accrete from the gas phase after it is formed by ion-molecule reactions (Scott et al. 1997). In hot core regions where elevated grain temperatures cause sublimation of the icy mantles, large gas phase abundances of ammonia have been found ($(1–10) \times 10^{-6}$ relative to hydrogen; Genzel et al. 1982; Blake et al. 1987; Heaton et al. 1989; Cesaroni et al. 1994). This considerably exceeds the abundance of NH_3 in cold dense regions ($N(NH_3)/N(H_2) \approx 10^{-7}$; Federman et al. 1990), indicating that the ices indeed form an important reservoir of NH_3.

The presence (or absence) of solid NH_3 has important implications for the chemistry of star forming regions. Whether in dense quiescent regions gaseous nitrogen will reside in its molecular or atomic form depends on the depletion of oxygen, since the reactions of atomic nitrogen with OH are an essential step towards N_2 formation (Charnley & Rodgers 2002). Thus the quantity of NH_3 that is present in the ices could give important information on the gas phase conditions of condensation. In addition, NH_3 can produce ions through acid-base chemistry under cryogenic conditions. This process likely explains the presence of OCN^- and probably $HCOO^-$ in interstellar ices (Grim & Greenberg 1987; Demyk et al. 1998; Novozamsky et al. 2002; Hudson et al. 2001; Keane et al. 2002). Finally, in the presence of NH_3, energetic processing of the ices by the ambient UV field could give rise to complex organic molecules, some of which could be of pre-biological significance, e.g., amino acids (Bernstein et al. 1995; Muñoz Caro et al. 2002; Bernstein et al. 2002; Muñoz Caro & Schutte 2003).

The main mid-infrared signatures of solid NH_3 are the umbrella mode at 9.0 μm, the NH stretching mode at 2.96 μm and the ammonium hydrate ($NH_3.H_2O$) feature at 3.48 μm. Searches for these bands are hampered by overlap with considerably stronger bands of other dust constituents. The 2.96 μm band overlaps with the strong 3 μm band of H_2O ice, the 9 μm band falls in the wing of the intense 9.7 μm silicate absorption, and the 3.48 μm feature is superimposed on the long wavelength shoulder of the 3 μm band. The non-detection of the 2.96 μm band as a substructure on the 3 μm feature mildly constrains the NH_3 abundance to $\lesssim$10% of H_2O when the ice in the line of sight is unannealed (Dartois et al. 2001; Smith et al. 1989; Gibb et al. 2001). However, for a considerable fraction of objects the ices in the line of sight are partially crystalline. In this case the upper limit is even less stringent, since crystalline H_2O ice produces a feature at 2.96 μm which is indistinguishable from the ammonia band (Gibb et al. 2001). In addition, the strength of the 2.96 μm band is considerably reduced when provisions are made for the effects of particle shapes (van der Bult et al. 1985; Smith et al. 1989).

Recently there have been a number of papers claiming the detection of the 9.0 μm umbrella mode of NH_3. Abundances

Send offprint requests to: W. A. Schutte,
e-mail: schutte@strw.leidenuniv.nl

⋆ Based on observations obtained at the European Southern Observatory (ESO), Paranal, Chile.

of up to 15% rel. to solid H_2O were inferred (Lacy et al. 1998; Gibb et al. 2000, 2001; Gürtler et al. 2002). However, such a detection is difficult, since it requires a reliable matching of the very strong underlying silicate feature. The profile of the silicate band varies between objects and so far no class of silicate materials has been found that consistently reproduces the 9.7 μm feature for embedded YSO's. Therefore, these studies relied on polynomial fitting of the silicate band. This technique has the clear drawback that it offers no guarantee for a robust match of the band profile underlying the broad NH_3 feature and therefore introduces the risk of a spurious detection. In addition, a comprehensive paper on this subject (Gibb et al. 2001) invoked a second, unidentified, feature centered at 9.2 μm to compensate for the poor match by the ammonia band of the absorption feature obtained after subtraction of the polynomial baseline. Clearly, independent confirmation of these detections is highly desirable.

Dartois & d'Hendecourt (2001) and Dartois et al. (2002), based on the weakness of the 3.48 μm feature of ammonium hydrate $NH_3.H_2O$ towards YSO's, derived NH_3 upper limits of less than 5%. Gibb et al. (2001) however argued that the $NH_3.H_2O$ feature is much broader than the observed 3.48 μm band and concluded that it could be part of the strong long wavelength shoulder of the 3 μm band, preventing significant constraints.

Traditionally observations of interstellar ices have been limited to the absorption features due to fundamental intramolecular vibrational transitions in the mid-IR region (2.5–20 μm). The vibrational overtones and combination bands fall in the near-IR (1–2.5 μm). These features are quite weak, with peak intensities of at most ~5% of those of the fundamentals. Observations of the near-IR bands of frozen molecules have been used for a long time to study the composition of the planets and satellites of the outer-solar system which are covered by thick layers of ice (e.g., Quirico et al. 1999). However, observations of interstellar ices are constrained by the amount of ice in the line of sight and the band strength therefore becomes a crucial factor. In addition, the near-IR region falls in the short wavelength tail of the emission by hot circumstellar dust where the flux drops very rapidly. Therefore, a meaningful search for interstellar ice features in the near-IR had to await the advent of 8 meter class telescopes like the Very Large Telescope (VLT).

The spectroscopic K-band which covers the 1.9–2.6 μm region provides a window for a number of near-IR features of ice components. First, NH_3 has a feature near 2.21 μm (Trotta & Schmidt 1994). Unlike its mid-IR features, this band is not overwhelmed by strong absorptions of other solids. Furthermore CH_3OH has a feature at 2.27 μm (Sect. 4.1 below). The presence of CH_3OH in the ices towards high mass YSO's has been firmly established from observations of a number of mid-IR absorption features (e.g., Dartois et al. 1999). Detection of the 2.27 μm band would therefore be an important test for the feasibility of observing interstellar ices in the near-IR and the consistency of the near-IR and mid-IR lines of sight. Finally H_2O ice gives two broad structures at 2 and 2.45 μm (e.g., Schmitt et al. 1998).

Due to its exceptionally high ice column density, the high mass embedded YSO W 33A has classically been the prime target to search for weak ice bands. This paper reports a search for the 2.21 and 2.27 μm bands towards W 33A with the the Infrared Spectrometer And Array Camera (ISAAC) at the Very Large Telescope (VLT) at Paranal, Chile. From these observations, in combination with laboratory experiments, we obtain stringent constraints on the abundance of solid NH_3 which contradict earlier estimates based on mid-IR observations.

2. Observations

2.1. Observations and data reduction

W 33A was observed on July 28 and September 22, 2001 with a total on-source integration time of 4800 s evenly distributed among the two nights. A 0″6 slit was used, which together with the low resolution grating on ISAAC gives an average resolution of $R = 750$. All spectra were obtained using a 15″ nod throw along the slit in a standard ABBA scheme with 150 s of integration time per frame. Each night a telluric standard star was observed before and after the observation of W 33A with an airmass difference of less than 0.05 in order to get the best cancellation of telluric lines. On the first night the telluric standards used were HD 91713 (K1III) and HD 175876 (O7V) while HD 154066 (B8V) and HD 161961 (B0.5III) were observed as standards during the second night. In the final spectrum HD 91713 was not used, since it did not have sufficiently high S/N and would thus only add noise to the combined spectrum of W 33A.

The frames were dark subtracted, flat fielded, distortion corrected and combined using the standard *eclipse* library. The spectra were then wavelength calibrated relative to a xenon arc lamp and flux calibrated relative to the standard stars.

Due to a strong reflection nebulosity around the primary source in W 33A, the extraction of a 1D spectrum has to be done with care. A pointlike source is clearly visible a few arcseconds to the south of the reflection nebula, which as expected is significantly more blue than the point source. The 1-dimensional spectrum of W 33A was extracted from a cross dispersion region centered on the point source with a width that maximizes the S/N ratio on the continuum of the extracted spectrum. The final spectrum has a S/N ratio of 150–200 at 2.1–2.4 μm.

The final spectrum was obtained by dividing each spectrum of W 33A by a standard star spectrum and combining the spectra from the two nights. A small shift of a fraction of a pixel was applied to the standard star spectra in order to optimize the telluric division. A very good cancellation of telluric features was achieved except in the 4900–5100 cm^{-1} region, where residuals from strong telluric absorption are still visible.

2.2. Spectrum

Figure 1 shows the observations. It can be seen that the spectrum is dominated by the exponentally rising continuum emission originating from the hot dust (~800–1000 K) close to the star while a number of relatively faint emission lines of

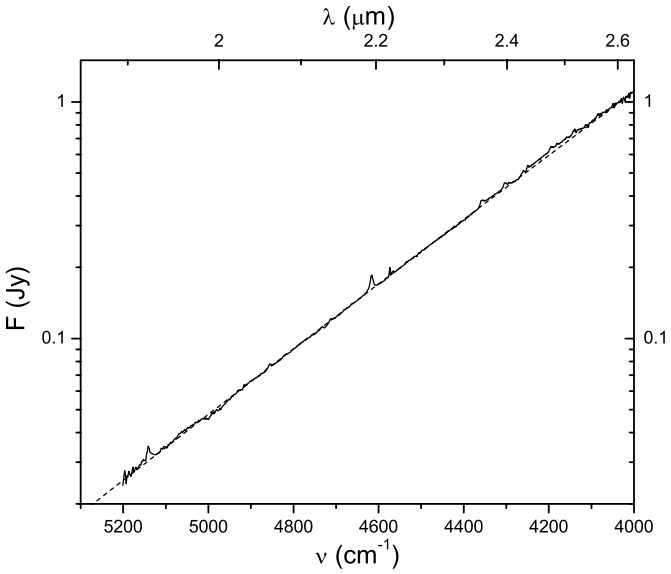

Fig. 1. *K* band spectrum of W 33A. The dashed line indicates the adopted continuum (see text).

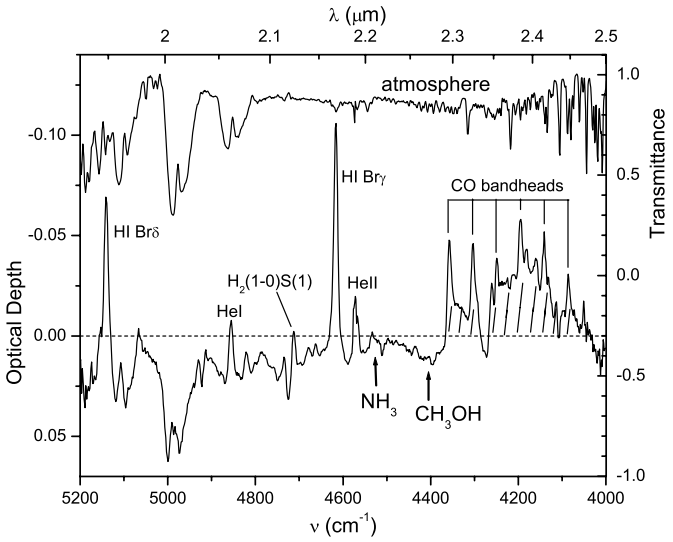

Fig. 2. Bottom curve: Optical depth spectrum of W 33A in the *K* band obtained by division with the adopted continuum (Fig. 1). The nature of the various emission bands is indicated. The arrows give the location of the 2.21 μm and 2.27 μm bands of NH_3 and CH_3OH, respectively. The top curve shows the atmospheric transmission at Paranal at the time of the observations.

circumstellar origin are superposed (see below). To enable a better search for minor absorption bands at the % level we divided by the indicated continuum. The continuum is given by a second order polynomial in the $\log(F)$ vs. ν plane which deviates only marginally from a straight line. The polynomial was defined by fitting the regions 4530–4500 cm^{-1} and 4040–4000 cm^{-1}. Other spectral regions either contain circumstellar emission features, or contain absorption bands of the various ice components towards W 33A (see Sect. 4 below).

The resulting optical depth spectrum is shown in Fig. 2. For comparison the atmospheric transmission in this region is also shown. The spectrum is dominated by a number of emission lines. Most prominent are the CO vibrational overtones between 2.3 and 2.6 μm, vibrational transitions of molecular hydrogen and the Brδ and Brγ hydrogen recombination lines at 1.947 μm and 2.166 μm, respectively. The presence of a significant population of H_2 in the second vibrational level and the CO bandheads indicate that the gas is hot (>2000 K), although the molecular hydrogen lines may be shock excited. Also, the fact that the CO lines are seen in emission shows that the gas is not placed in front of the infrared continuum source, but may be part of a nearly face-on circumstellar disk (e.g. Najita et al. 1996; Carr et al. 2001).

The hydrogen recombination lines are often interpreted as being a sign of accretion activity and in the case of high mass young stars they may originate in an ionized wind (e.g. Nisini et al. 1995). In this case the lines are formed within a few stellar radii of the star itself. In the case of a massive star like W 33A the lines may also be formed in the associated HII region, since the line-to-continuum ratio varies with more than an order of magnitude throughout the nebulosity in the cross dispersion direction. This clearly indicates that the hydrogen emission is not scattered from the inner regions of the source along with the continuum emission, but is rather produced where it is observed. On the other hand the line-to-continuum ratio of the CO lines seems to be constant on all positions along the slit, indicating that this emission is indeed scattered along with the continuum emission and is thus produced close to the source. The H_2 lines are unfortunately too weak to be clearly detected in the reflection nebulosity.

It can be seen that a shallow absorption band appears at 2.27 μm. In addition a broad absorption feature may be present between 1.92–2.12 μm. An apparent absorption structure at 2 μm is caused by residual telluric structure.

2.3. Line-of-sight effects

It can be argued that if the emission towards W 33A in the *K*-band is due to scattered light, a different line of sight may be probed than at mid-infrared wavelengths. We have tested this possible difficulty by comparing our *K*-band acquisition image to a 3.3 μm image which was obtained during the same observation run. Astrometry relative to 4 nearby stars constrain the positions of the W 33A point source at 2.2 μm and 3.3 μm to differ by less than 0″3. This indicates that the lines of sight probed are identical within 1100 AU, assuming a distance of 3.7 kpc (Wynn-Williams 1982). This distance may still be enough to cause significant differences in observed abundances, since the small scale distribution of ices around young stars is largely unknown. E.g. adaptive optics *K*-band spectroscopy is necessary to further constrain the effects of differing lines of sight due to scattering. However, as will be discussed in Sects. 5 and 6, column densities of tracer species such as CH_3OH and CO_2 appear to be invariant between the near- and mid-IR, indicating that such line of sight effects are likely negligible.

3. Experimental

A detailed description of the procedure used for the creation and analysis by infrared spectroscopy of simulated interstellar

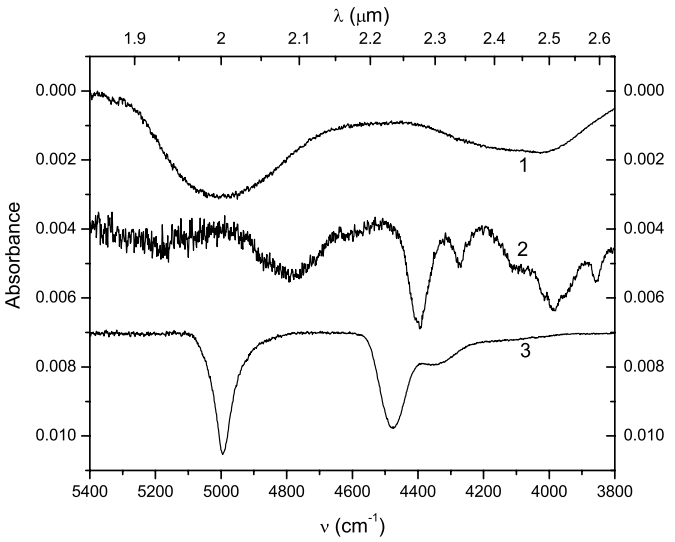

Fig. 3. Near-IR spectra of 1. H_2O; 2. CH_3OH and 3. NH_3. All spectra correspond with pure ices at 12 K.

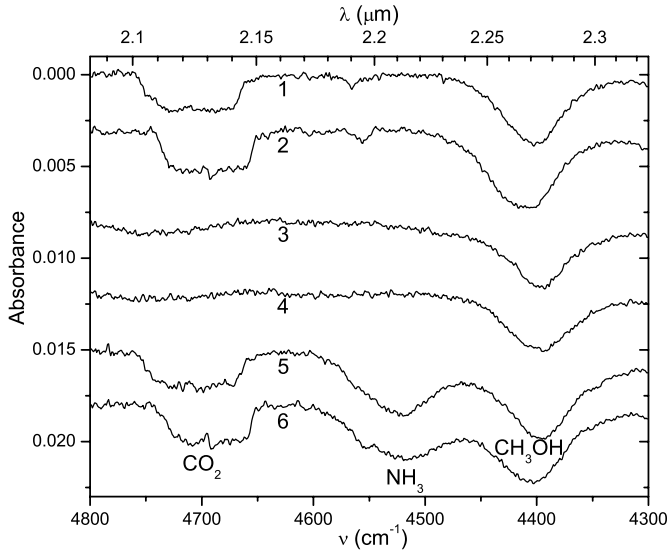

Fig. 4. The 2.27 μm CH_3OH feature in different ice mixtures:
1. H_2O : CH_3OH : CO_2 = 1 : 0.7 : 1 (120 K).
2. H_2O : CH_3OH : CO_2 = 1 : 0.7 : 1 (12 K)
3. CH_3OH (120 K)
4. CH_3OH (12 K)
5. H_2O : CH_3OH : CO_2 : NH_3 = 1 : 0.8 : 1 : 0.3 (120 K)
6. H_2O : CH_3OH : CO_2 : NH_3 = 1 : 0.8 : 1 : 0.3 (12 K).
The spectra have been offset for clarity.

ice samples was published earlier (Gerakines et al. 1995). The samples were deposited at 12 K followed by a step-wise warm-up while monitoring the evolution of the infrared spectrum.

The reagents used in these experiments were H_2O liquid (purified by three freeze-thaw cycles), CO_2 gas (Praxair, 99.996% purity), NH_3 gas (Praxair, 99.99% purity) and CH_3OH liquid (Janssen Chimica, 99.9% purity). For samples containing both NH_3 and CO_2, NH_3 was deposited through a separate tube, to prevent reactions prior to deposition.

4. Experimental results

Figure 3 gives the spectra of solid NH_3, CH_3OH and H_2O over the entire near-IR region. It can be seen that NH_3 produces two sharp features, near 2.00 and 2.21 μm. However, the stronger 2.00 μm feature falls in a region of very poor atmospheric transmission (Fig. 2). CH_3OH shows a variety of structures. Apart from the 2.27 μm band, these are shallow and fall in regions that are crowded with atmospheric lines or circumstellar emission bands (Fig. 2). H_2O gives 2 broad features, at 2.0 and 2.45 μm, where the latter is quite weak.

We studied the spectra of the 2.27 μm CH_3OH and 2.21 μm NH_3 bands as well as the broad feature of amorphous H_2O ice around 2 μm in a variety of ice mixtures. Three different kind of mixtures were used: ices dominated by H_2O, ices in which H_2O, CO_2 and CH_3OH are present in similar abundances, and finally the pure ices. The mixtures are thought to be representative of the composition of interstellar ices in various dense regions (Dartois et al. 1999; Gerakines et al. 1999; Ehrenfreund et al. 1999). The pure samples were studied for comparison.

4.1. CH_3OH

Figure 4 presents 4800-4300 cm^{-1} spectra of the ice mixtures H_2O : CH_3OH : CO_2 = 1 : 0.7 : 1, H_2O : CH_3OH : CO_2 : NH_3 = 1 : 0.8 : 1 : 0.3 as well as pure CH_3OH at 12 K and 120 K showing the 2.27 μm feature of CH_3OH. The width and position of this band depends somewhat on temperature and composition (Fig. 4). The position varies between 4410 and 4395 cm^{-1}, and $FWHM$ varies between 55–65 cm^{-1}. Besides the CH_3OH feature, the spectra also show the NH_3 band at 2.21 μm (Sect. 4.2) and a feature at 2.13 μm caused by CO_2.

We measured the band strengths of the 2.27 μm band at different temperatures (see Table 1). These were obtained by comparison with mid-IR features of known intensity, using:

$$A_2(T_2) = \frac{\int \tau_2(T_2)\mathrm{d}\nu}{\int \tau_1(T_1)\mathrm{d}\nu} A_1(T_1) \quad (1)$$

here subscript 1 and 2 refer to mid- and near-IR, respectively, A is the band strength of the feature, $\int \tau(T)\mathrm{d}\nu$ its integrated optical depth, and T is the ice temperature. Equation (1) holds as long as no sublimation occurs in the temperature interval T_1–T_2. The mid-IR band strengths for methanol and ammonia in various mixtures after deposition at 12 K were obtained from Kerkhof et al. (1999; see Table 1).

4.2. NH_3

Figure 5 shows the 2.21 μm ammonia feature for a number of mixtures, H_2O : CH_3OH : CO_2 : NH_3 = 1 : 0.8 : 1 : 0.3, H_2O : NH_3 = 10 : 1.4 and pure NH_3. The position is almost the same for all mixtures, around 4525 cm^{-1}, while the pure ammonia feature falls at 4480 cm^{-1}. The $FWHM$ varies between 45–70 cm^{-1} for the matrices. For pure ammonia, the width is ~85 cm^{-1}. The band strength for the 2.21 μm feature was calculated with the procedure described in Sect. 4.1 (see Table 1).

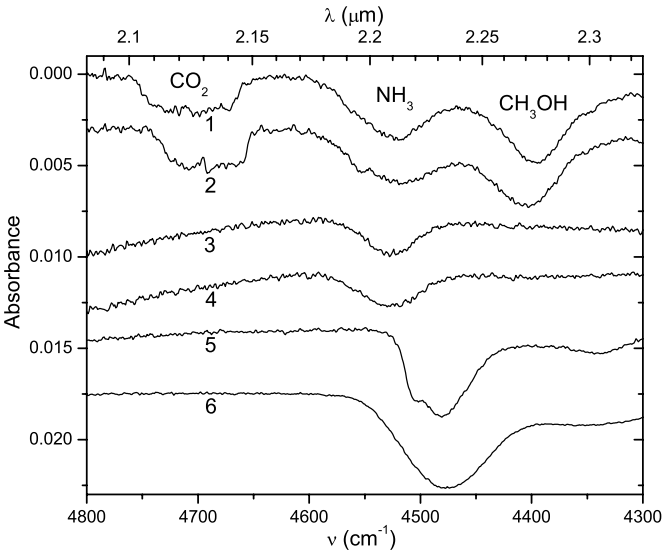

Fig. 5. The 2.21 μm NH_3 feature in different ice mixtures:
1. H_2O : CH_3OH : CO_2 : NH_3 = 1 : 0.8 : 1 : 0.3 (120 K)
2. H_2O : CH_3OH : CO_2 : NH_3 = 1 : 0.8 : 1 : 0.3 (12 K)
3. H_2O : NH_3 = 10 : 1.4 (120 K)
4. H_2O : NH_3 = 10 : 1.4 (12 K)
5. NH_3 (120 K)
6. NH_3 (12 K).
The spectra have been offset for clarity.

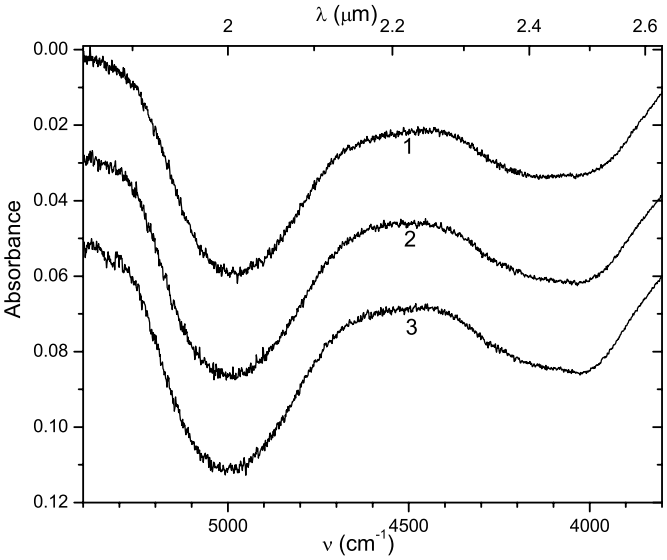

Fig. 6. Spectra of pure H_2O ice at 1. 120 K, 2. 50 K, 3. 12 K. The spectra have been offset for clarity.

4.3. H_2O

The near-IR spectrum of pure H_2O ice after deposition at 12 K and warm-up to 50 and 120 K is shown in Fig. 4. The band strength was derived following the method described in Sect. 4.1 (see Table 1).

5. Comparison to observations

Figure 7 compares the W 33A spectrum to H_2O : CH_3OH : CO_2 = 1 : 0.7 : 1 (at 120 K) and H_2O : NH_3 = 10 : 1.4

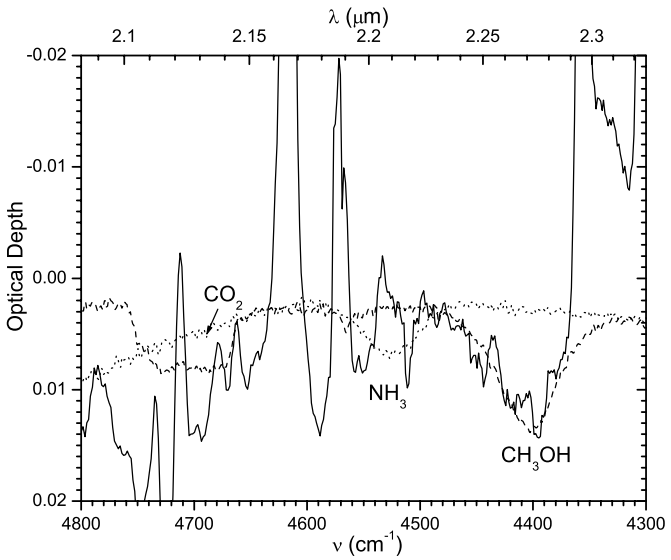

Fig. 7. The optical depth spectrum of W 33A compared with H_2O : CH_3OH : CO_2 = 1 : 0.7 : 1 at 120 K (dashed line) and H_2O : NH_3 = 10 : 1.4 at 50 K (dotted line). The NH_3 2.21 μm feature in the laboratory spectrum has been scaled to the maximum intensity consistent with its non-detection towards W 33A.

(at 50 K). Temperatures were selected according to the temperatures which have been derived from the ice features in the mid-IR, e.g., solid CH_3OH shows $T \approx 116$ K (Gerakines et al. 1999; Ehrenfreund et al. 1999). No direct observations are available for the water 3 μm feature, because it is saturated for W 33A. However, observations of this feature towards other high mass young stellar objects give temperatures in the range 20–70 K (Smith et al. 1989). Therefore, we used 50 K for water-dominated ices when matching these to the W 33A spectrum.

The methanol feature in Fig. 7 gives a good match to the shallow 2.27 μm absorption band in the W 33A spectrum. Table 2 lists the implied CH_3OH column density. The value of 1.8×10^{18} cm^{-2} is in excellent agreement with the column density of 1.85×10^{18} cm^{-2} obtained from the methanol features at 3.54 and 3.91 μm (Dartois et al. 1999). To assess the robustness of this result, we also list the column densities which were obtained by matching the observations to the methanol feature in the other laboratory mixtures, giving similar results. The match was less favorable for these other mixtures. This agrees well with the results from the mid-IR, which showed that ices containing similar abundances of CH_3OH, CO_2 and H_2O give the best matches to the methanol features (Dartois et al. 1999; Ehrenfreund et al. 1999).

Figure 7 shows that there is no indication of the presence of the 2.21 μm NH_3 feature in the W 33A spectrum. Using the H_2O : NH_3 = 10 : 1.4 ice spectrum, we estimate an upper limit of $\tau(2.21) \leq 0.004$ (Fig. 6). This band depth is constrained by the 3 σ noise level from 2.220–2.227 μm (4505–4490 cm^{-1}), a clear spectral region free of emission and absorption bands. With the band strength from Table 1, the upper limit yields $N(NH_3) < 6.1 \times 10^{17}$ cm^{-2}. Comparison with the spectra of the other two mixtures gave similar upper

Table 1. Band strengths for CH_3OH 2.27 μm, NH_3 2.21 μm and H_2O 2.0 μm bands. The mid-IR modes used for calibration are listed.

Ice Mixture				Molecule	T	ν	λ	A(near-IR)	mid-IR mode	A(mid-IR[a])
H_2O	CH_3OH	CO_2	NH_3		K	cm^{-1}	μm	cm molecule^{-1}		cm molecule^{-1}
1	0.8	1	0.3	CH_3OH	12	4404	2.271	6.5×10^{-19}	C-O stretching	1.9×10^{-17}
					120	4398	2.274	7.9×10^{-19}		
				NH_3	12	4517	2.214	1.3×10^{-18}	umbrella	2.2×10^{-17}
					120	4521	2.212	1.4×10^{-18}		
1	0.7	1		CH_3OH	12	4410	2.268	5.2×10^{-19}	C-O stretching	1.9×10^{-17}
					120	4407	2.269	4.4×10^{-19}		
10			1.4	NH_3	12	4528	2.208	4.8×10^{-19}	umbrella	1.3×10^{-17}
					50	4527	2.209	5.1×10^{-19}		
			1	NH_3	12	4478	2.233	9.7×10^{-19}	umbrella	1.7×10^{-17}
					50	4481	2.232	8.4×10^{-19}		
	1			CH_3OH	12	4395	2.275	5.9×10^{-19}	C-O stretching	1.8×10^{-17}
					50	4394	2.276	6.6×10^{-19}		
1				H_2O	12	4998	2.001	1.1×10^{-18}	O-H stretching	2.0×10^{-16}
					50	4998	2.001	1.2×10^{-18}		

[a] From Kerkhof et al. (1999), intensity is somewhat dependent on matrix.

Table 2. Ammonia limits and methanol abundances relative to water.

Ice mixture				Molecule	τ_{int}	N	$N/N(H_2O)$	Temperature
H_2O	CH_3OH	CO_2	NH_3		(cm^{-1})	(cm^{-2})	%	(K)
1	0.8	1	0.3	NH_3	<0.60	$<4.3 \times 10^{17}$	<3.6	120
10			1.4	NH_3	<0.31	$<6.1 \times 10^{17}$	<5.0	50
			1	NH_3	<0.60	$<7.1 \times 10^{17}$	<5.9	50
1	0.7	1		CH_3OH	0.8	1.8×10^{18}	15	120
1	0.8	1	0.3	CH_3OH	1.5	1.9×10^{18}	16	120
	1			CH_3OH	1.2	1.8×10^{18}	14	50

limits (Table 2), showing that the amount of solid NH_3 is <5% of H_2O.

While theoretically it is possible that there would be an emission band in the 2.220–2.227 μm region which would exactly cancel out an absorption band due to NH_3, the likelihood of such a phenomenon seems small. Indeed there are 10 data points in this interval, and none shows a non-statistical deviation from the smooth overall spectral behaviour in this region. Higher resolution spectroscopy could provide a decisive test of this issue.

It is unlikely that the 2.13 μm feature of CO_2 can be detected towards W 33A. While in the laboratory sample in Fig. 6 CO_2:CH_3OH = 0.7:1, the relative column densities towards W 33A give CO_2:CH_3OH = 1:0.7 (Gibb et al. 2001). Therefore it is expected that for W 33A, relative to the CH_3OH 2.27 μm feature, the 2.13 μm band would be 2 times weaker than in the laboratory sample. Figure 6 indicates that such a band would be undetectable.

Finally, Fig. 8 compares the 2 μm water feature to the W 33A spectrum. The laboratory feature has been scaled to the column density derived from the mid-IR spectrum (1.2×10^{19} cm^{-2}; Gibb et al. 2000; Schutte et al. 2002). It is clear that, while the observed spectrum is consistent with the presence of the 2 μm feature, a positive detection of this feature is hampered by the strong telluric structure between 5200–4800 cm^{-1}.

6. Astrophysical implications

The column density of CH_3OH derived from the 2.27 μm feature agrees with that derived from the mid-IR absorption bands. The same kind of agreement was also observed for the 2.7, 4.2 and 15.2 μm features of CO_2 towards various other sources (Gerakines et al. 1999; Keane et al. 2001). This indicates that the mid- and near-IR photons trace the same line of sight.

On the other hand, the NH_3 upper limit of 5.9×10^{17} cm^{-2} (<5% of solid H_2O) derived from the absence of the 2.21 μm feature is a factor 3 lower than the previously reported column density $N(NH_3)$ = 1.7 × 10^{18} cm^{-2} (Gibb et al. 2000, 2001; Gürtler et al. 2002). It agrees with the general upper limit of ~5% derived by Dartois & d'Hendecourt (2001) and Dartois et al. (2002) from the 3.47 μm ammonium hydrate feature. We note that the current determination is more direct and does not suffer from any baseline ambiguities which could have influenced this earlier determination (Gibb et al. 2001). We attribute the discrepancy between the present upper limit and the column density from Gibb et al. to the large uncertainty in the baseline definition in the region of the 9 μm umbrella mode which falls inside the intense silicate absorption feature (see

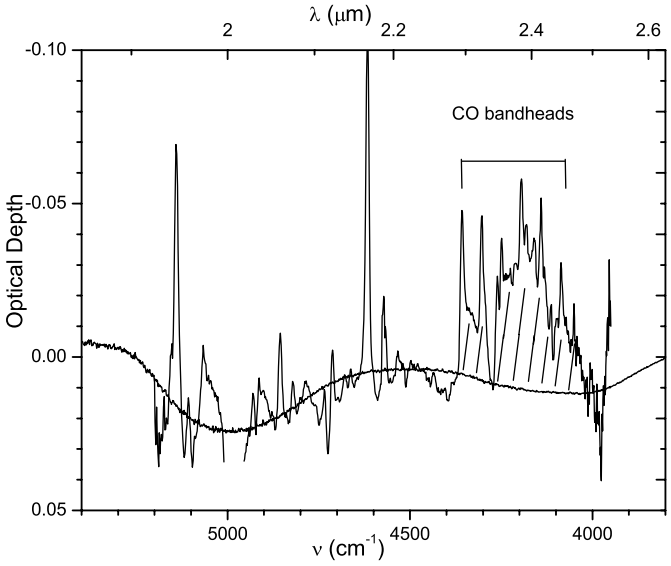

Fig. 8. The optical depth spectrum of W 33A compared to pure water ice at 50 K. The laboratory spectrum was scaled to correspond to the H_2O column density towards W 33A (see text). Parts of the spectral region in which the atmospheric transmission is less than 0.7 are omitted.

discussion Sect. 1). While our result reveals such a discrepancy only for W 33A, similar problems may apply to *all* prior determinations of the NH_3 abundance towards YSO's based on the umbrella mode. We thus conclude that the abundance of solid NH_3 may have been considerably overestimated in general, and that, except for W 33A, no stringent limits to its abundance are available at this time.

Further observations of the NH_3 2.21 μm band are essential to investigate the role of NH_3 in interstellar ices. Another object which is a prime target for observing the 2.21 μm feature is NGC 7538:IRS9, for which an NH_3 abundance of ~10% has been reported based on the possible detection of the umbrella mode (Lacy et al. 1998; Gibb et al. 2001; Gürtler et al. 2002).

In view of the stringent upper limit for NH_3, other species must contain most of the nitrogen in the ices towards W 33A. A good candidate is the infrared inactive molecule N_2. On the other hand, NH_3 could have initially accreted, but may have been converted to other species by subsequent chemistry. Such a species could be the NH_4^+ ion, whose presence seems to be indicated by the 6.85 μm ice absorption band observed towards embedded YSO's (Grim et al. 1989; Schutte & Khanna 2003). In any case, the present result gives essential new insight in the form in which nitrogen is included in the icy grain mantles near young stellar objects and therefore gives important constraints to our understanding of the chemical conditions of star formation.

Acknowledgements. We thank Louis d'Hendecourt and Emmanuel Dartois for their scientific advice and stimulating discussions.

References

Bernstein, M. P., Sandford, S. A., Allamandola, L. J., Chang, S., & Scharberg, M. A. 1995, ApJ, 454 327
Bernstein, M. P, Dworkin, J. P., Sandford, S. A., Cooper, G. W, & Allamandola, L. J. 2002, Nature, 416, 401
Blake, G. A., Sutton, E. C., Masson, C. R., & Phillips, T. G. 1987, ApJ, 315, 621
Carr, J. S., Mathieu, R. D., & Najita, J. R. 2001, ApJ, 551, 454
Charnley, S. B., & Rodgers, S. D. 2002, ApJ, 569, L133
Cesaroni, R., Churchwell, E., Hofner, P., Walmsley, C. M., & Kurtz, S. 1994, A&A, 288, 903
Dartois, E., Schutte, W. A., Geballe, T. R., et al. 1999, A&A, 342, L32
Dartois, E., & d'Hendecourt, L. 2001, A&A, 365, 144
Dartois, E., d'Hendecourt, L., Thi, W., Pontoppidan, K. M., & van Dishoeck, E. F. 2002, A&A, 394, 1057
Demyk, K., Dartois, E., d'Hendecourt, L., et al. 1998, A&A, 339, 553
Ehrenfreund, P., Kerkhof, O., Schutte, W. A., et al. 1999, A&A, 350, 240
Federman, S. R., Huntress, Jr. W. T., & Prasad, S. S. 1990, ApJ, 479, 818
Genzel, R., Ho, P. T. P., Bieging, J., & Downes, D. 1982, ApJ, 259, L103
Gerakines, P. A., Schutte, W. A., Greenberg, J. M., & van Dishoeck, E. F. 1995, A&A, 296, 810
Gerakines, P. A., Whittet, D. C. B., Ehrenfreund, P., et al. 1999, ApJ, 522, 357
Gibb, E. L., Whittet, D. C. B., & Chiar, J. E. 2001, ApJ, 558, 702
Gibb, E. L., Whittet, D. C. B., Schutte, W. A., et al. 2000, ApJ, 536, 347
Grim, R. J. A., & Greenberg, J. M. 1987, ApJ, 321, L91
Grim, R. J. A., Greenberg, J. M., Schutte, W. A., & Schmitt, B. 1989, ApJ, 341, L87
Gürtler, J., Klaas, U., Henning, Th., et al. 2002, A&A, 390, 1075
Heaton, B. D., Little, L. T., & Bishop, I. S. 1989, A&A, 213, 148
Hiraoka, K., Yamashita, A., Yachi, Y., et al. 1995, ApJ, 443, 363
Hudson, R. L., Moore, M. H., & Gerakines, P. A. 2001, ApJ, 550, 1140
Keane, J. V., Boogert, A. C. A, Tielens, A. G. G. M., Ehrenfreund, P., & Schutte, W. A. 2001, A&A, 375, L43
Keane, J. V., Schutte, W. A., & Tielens, A. G. G. M. 2002, A&A, in press
Kerkhof, O., Schutte, W. A., & Ehrenfreund, P. 1999, A&A, 346, 990
Lacy, J. H., Faraji, H., Sandford, S. A., & Allamandola, L. J. 1998, 501, L105
Muñoz Caro, G. M., Meierhenrich, U. J., & Schutte, W. A. 2002, Nature, 416, 403
Muñoz Caro, G. M., & Schutte, W. A. 2003, A&A, submitted
Najita, J., Carr, J. S., Glassgold, A. E., Shu, F. H., & Tokunaga, A. T 1996, ApJ, 462, 919
Nisini, B., Milillo, A., Saraceno, P., & Vitali, F. 1995, A&A, 302, 169
Novozamsky, J. H., Schutte, W. A., & Keane, J. V. 2002, A&A, 379, 588
Quirico, E., Douté, S., Schmitt, B., et al. 1999, Icarus, 139, 157
Schmitt, B., Quirico, E., Trotta, F., & Grundy, W. M. 1998, in Solar System Ices, ed. B. Schmitt, M. Festou, & C. deBergh (Kluwer Academic, Dordrecht), 199
Schutte, W. A. 1999, in Laboratory Astrophysics and Space Research, ed. P. Ehrenfreund, C. Krafft, H. Kochan, & V. Pirronello (Kluwer Academic, Dordrecht), 69
Schutte, W. A., & Khanna, R. K. 2003, submitted to A&A
Scott, G. B. I., Freeman, C. G., & McEway, M. J. 1997, MNRAS, 290, 636
Smith, R. G., Sellgren, K., & Tokunaga, A. T. 1989, ApJ, 344, 413
Trotta, F., & Schmitt, B. 1994, in AIP Conf. Proc. 312, Molecules and Grains in Space, ed. I. Nenner (AIP press, New York), 759
van de Bult, C. E. P. M., Greenberg, J. M., & Whittet, D. C. B. 1985, MNRAS, 214, 289
Wynn-Williams, C. G. 1982, ARA&A, 20, 587